

Ribonuclease Activity of Vaccinia DNA Topoisomerase IB: Kinetic and High-Throughput Inhibition Studies Using a Robust Continuous Fluorescence Assay[†]

Keehwan Kwon, Rajesh Nagarajan, and James T. Stivers*

Department of Pharmacology and Molecular Sciences, The Johns Hopkins University School of Medicine,
725 North Wolfe Street, Baltimore, Maryland 21205-2185

Received June 9, 2004; Revised Manuscript Received September 18, 2004

ABSTRACT: Vaccinia type I DNA topoisomerase exhibits a strong site-specific ribonuclease activity when provided a DNA substrate that contains a single uridine ribonucleotide within a duplex DNA containing the sequence 5' CCCTU 3'. The reaction involves two steps: attack of the active site tyrosine nucleophile of topo I at the 3' phosphodiester of the uridine nucleotide to generate a covalent enzyme–DNA adduct, followed by nucleophilic attack of the uridine 2'-hydroxyl to release the covalently tethered enzyme. Here we report the first continuous spectroscopic assay for topoisomerase that allows monitoring of the ribonuclease reaction under multiple-turnover conditions. The assay is especially robust for high-throughput screening applications because sensitive molecular beacon technology is utilized, and the topoisomerase is released during the reaction to allow turnover of multiple substrate molecules by a single molecule of enzyme. Direct computer simulation of the fluorescence time courses was used to obtain the rate constants for substrate binding and release, covalent complex formation, and formation of the 2',3'-cyclic phosphodiester product of the ribonuclease reaction. The assay allowed rapid screening of a 500 member chemical library from which several new inhibitors of topo I were identified with IC₅₀ values in the range of 2–100 μ M. Three of the most potent hits from the high-throughput screening were also found to inhibit plasmid supercoil relaxation by the enzyme, establishing the utility of the assay in identifying inhibitors of the biologically relevant DNA relaxation reaction. One of the most potent inhibitors of the vaccinia enzyme, 3-benzo[1,3]dioxol-5-yl-2-oxoproprionic acid, did not inhibit the closely related human enzyme. The inhibitory mechanism of this compound is unique and involves a step required for recycling the enzyme for steady-state turnover.

Type IB DNA topoisomerases (topo I) catalyze the reversible cleavage of the phosphodiester backbone of DNA using a nucleophilic active site tyrosine residue (1). In the normal reaction, the DNA 5'-hydroxyl serves either as the leaving group during nucleophilic attack by the tyrosine or as the nucleophile in the reverse reaction in which the tyrosine is expelled, and the DNA backbone is religated (Figure 1A). As with many enzymes, the active site of topo I exhibits plasticity and allows alternative reactions to occur with remarkable catalytic promiscuity (2). These reactions include DNA strand exchange (3), attack of the phosphotyrosine intermediate by exogenous small molecule nucleophiles such as hydrogen peroxide and glycerol (4, 5), and a ribonuclease (RNase)¹ activity in which the tyrosine attacks the 3' phosphodiester linkage of a single ribonucleotide in an otherwise DNA context (6). In the ribonuclease reaction (Figure 1B), the 5'-hydroxyl of the DNA and the 2'-hydroxyl of the ribonucleotide compete for attack at the phosphotyrosine

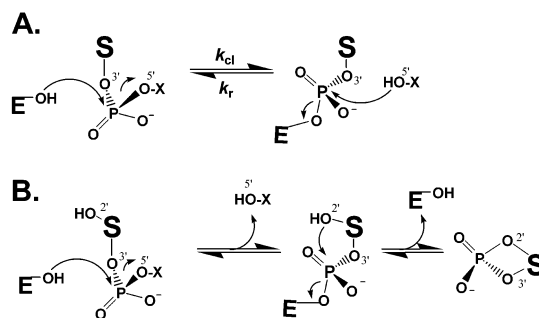


FIGURE 1: Topo I catalyzed reactions. (A) The reversible site-specific cleavage and ligation reaction in which the nucleophilic tyrosine attacks a DNA phosphodiester linkage, expelling a 5'-hydroxyl leaving group. (B) The irreversible ribonuclease reaction in which the enzyme attacks the 3'-phosphodiester linkage of uridine within the consensus sequence 5'-CCCTU-3'. The phosphotyrosine intermediate is then attacked by the 2'-hydroxyl group, resulting in turnover of the enzyme and formation of a cyclic 2',3'-phosphodiester product.

[†] This work was supported by National Institutes of Health Research Grant GM 68626 (to J.T.S.).

* To whom correspondence should be addressed. Tel: 410-502-2758. Fax: 410-955-3023. E-mail: jstivers@jhmi.edu.

¹ Abbreviations: vTopo, vaccinia DNA topoisomerase IB; hTopo, human topoisomerase IB; FAM, 6-carboxyfluorescein; P, 2-aminopurine; RNase, ribonuclease; buffer A, 20 mM Tris-HCl and 200 mM NaCl, pH 9.0.

linkage, leading to either religation of DNA or irreversible formation of a 2',3'-cyclic phosphodiester (Figure 1B).

The type IB enzyme isolated from vaccinia virus has a unique and robust site-specific RNase activity that mimics the specificity of the normal DNA cleavage activity of the enzyme (6). The vaccinia topo I cleaves DNA at the 3'

Here we report a new multiple-turnover kinetic assay for topo I that takes advantage of molecular beacon technology and the ribonuclease activity of the enzyme (Figure 2). Molecular beacons are DNA duplexes that have a fluorophore and quench positioned in molecular contact with each other, usually by covalent attachment at the 3' and 5' ends of a duplex DNA (12, 13). Thus, the duplex is nonfluorescent in the initial state, but when the covalent nature of the DNA backbone is disrupted by topo I phosphodiester cleavage, the small strand containing the fluorophore can spontaneously dissociate, leading to a large increase in fluorescence. If the substrate contains a ribonucleotide, the covalently attached enzyme can be released for multiple turnovers by attack of the 2'-hydroxyl group. This assay is used in a complete mechanistic analysis of the topo I RNase activity and to rapidly identify novel enzyme inhibitors from a 500 member chemical library.

Enzymes and Plasmid DNA. The cloning and purification of wild-type and Y274F vaccinia topoisomerase have been previously described (14). The enzyme concentration was determined by UV absorbance using an extinction coefficient of $28140 \text{ M}^{-1} \text{ cm}^{-1}$ in a buffer containing 20 mM sodium phosphate, pH 6.0, and 6 M guanidine hydrochloride (14). Human topoisomerase was obtained from Sigma. The plasmid pUC19/AID was constructed from pUC19 by inserting the 600 bp gene encoding the enzyme activation induced cytidine deaminase (AID) into the restriction sites *Nde*I and *Hind*III.

18U-FAM/18-DAB 5' CGTGTCGCCCTUATTCCG-FAM-3'
3' GCACAGCGGGAATAAGGC-DAB-5'

label, and second, the nucleotide just 3' of the ultimate T of the pentameric consensus sequence (underlined) was labeled with the fluorescent adenine analogue, 2-aminopurine (P). These two probes allowed (i) measurement of protein binding by monitoring the increase in fluorescein anisotropy of the DNA and (ii) DNA cleavage by the increase in 2-aminopurine fluorescence when the 6 mer leaving group rapidly dissociates after strand scission (14). The oligonucleotide strands were synthesized using an ABI 394 synthesizer using nucleoside phosphoramidites obtained from Glen Research. The oligonucleotides were purified using anion-exchange HPLC and desalted using disposable gel filtration columns (PD-10, Pharmacia). The purity of oligonucleotides was confirmed using electrophoresis through a 20% polyacrylamide gel containing 7 M urea and MALDI-TOF analysis. The DNA duplexes were prepared in buffer A (20 mM Tris-HCl and 200 mM NaCl, pH 9.0) by mixing the two strands in a molar ratio of 1.1 to 1 (the dabcyI-labeled strand was in slight molar excess).

Steady-State Fluorescence Emission Spectroscopy. Fluorescein fluorescence emission spectra of 18U-FAM/18-DAB were collected using a Fluoromax-3 fluorometer (Instruments S.A., Inc.) at 37 °C. The measurements were performed using an excitation wavelength of 492 nm, and the emission was monitored from 510 to 620 nm. The excitation and emission slit widths were set at 0.5 and 5 nm, respectively. Further experimental details are reported in the legend to Figure 2.

Steady-State Fluorescence Anisotropy Measurements. Samples (150 μL containing 0.1 μM FAM-18AP/24) were excited with vertically polarized light at 492 nm (1 nm band-pass), and both vertical and horizontal emissions were monitored at 517 nm (3 nm band-pass). Three replicate measurements were made for each addition of topoisomerase in the range 0–2.5 μM , and the values were then averaged. The G factor was calculated, and its value was used to calculate the anisotropy. The equilibrium dissociation constant was calculated by nonlinear least-squares fitting of the data to the equation

$$A = A_o - ((A_o - A_f)/2[\text{DNA}]_{\text{tot}}\{b - \sqrt{b^2 - 4[\text{E}]_{\text{tot}}[\text{DNA}]_{\text{tot}}}\}) \quad (1)$$

where A is the fluorescence anisotropy at a given concentration of vTopo, A_o and A_f are the anisotropies of the free DNA and the vTopo–DNA complex, and $[E]_{\text{tot}}$ and $[DNA]_{\text{tot}}$ are the total concentrations of DNA and vTopo. To determine whether **112983** displaced the bound DNA from Y274F, a complex was formed using 0.1 μM FAM-18AP/24 and 2 μM Y274F, and the anisotropy was measured as increasing concentrations of **112983** were added to the solution (0–28 μM). Anisotropy measurements were carried out in triplicate and the results averaged.

Kinetic Measurements of *v*Topo RNase Activity. Reactions (150 μ L) were performed in buffer A at 37 °C using 10 nM *v*Topo and substrate concentrations of 0.05, 0.1, 0.2, 0.4, and 0.8 μ M. Reactions were initiated by the addition of 2 μ L of a concentrated *v*Topo solution to the 18U-FAM/18-DAB substrate and buffer. After mixing, the increase in fluorescence intensity at 517 nm with excitation at 492 nm was followed for 3600 s. The excitation and emission slit widths were set at 0.5 and 5 nm, respectively. Time points were collected at 1 s intervals with an integration time of 1 s. Raw fluorescence readings were converted to product concentration using the equation

$$[P]_t = [S]_{\text{tot}}(F_t - F_0)/(F_{\text{max}} - F_0) \quad (2)$$

and the data were fitted by computer simulation to the mechanism shown in Scheme 1 (see Results and Discussion) using the program Dynafit (15). In this equation F_0 is the initial fluorescence, F_t is the measured fluorescence at time t , and F_{max} is the fluorescence after complete conversion of substrate to product. The results reported in Table 1 are the average obtained from two experiments such as that shown in Figure 3A.

High-Throughput Inhibition Studies. For screening of the NCI Diversity Library, a Fluoromax-3 fluorometer with a MicroMax 96-well fluorescence plate reader attachment was utilized. In our initial studies, five plates from the library were screened (3843–3847), comprising 480 unique compounds. Each reaction well in the screen contained enough test compound to give a 100 μ M solution after addition of 200 μ L of reaction solution containing enzyme (10 nM) and buffer A. Reactions were then initiated by the addition of 18U-FAM/18-DAB (0.5 μ M final concentration in the well). For validation, positive and negative control wells were also included that consisted of enzyme and substrate without inhibitor and of substrate without enzyme. The rates of fluorescence change at 517 nm with excitation at 492 nm were followed by taking three fluorescence readings in each well over a 30 min time period.

Inhibition of the *v*Topo RNase Activity by **112983.** To determine the inhibition mechanism of the best inhibitor **112983**, the concentration dependence of RNase inhibition was studied at two concentrations of 18U-FAM/18-DAB equal to about $1/6$ th and 10 times the K_m . These two substrate concentrations allow determination of whether the inhibition is competitive or, alternatively, involves a ternary complex between the enzyme, substrate, and inhibitor. The **[112983]** was varied in the range 0–32 μ M, and the fluorescence changes as a function of time were monitored using the MicroMax plate reader as described above. Global kinetic fitting of the product formation curves was used to determine the K_i for inhibition by **112983** using the program Dynafit (15). The inhibition experiment with **112983** was repeated a total of three times using both 50 nM and 3 μ M *v*Topo RNase substrate. The error in the reported K_i reflects the errors in the individual simulations.

Inhibition of Steady-State Plasmid Supercoil Relaxation. Supercoil relaxation reactions were performed with 100 nM supercoiled pUC19/AID, 3 nM *v*TOPO or two units of hTopo, and various concentrations of inhibitor. The reaction mixtures were incubated for 9 min (15 min for hTopo) at room temperature and were then quenched with 1 volume

of loading buffer containing 0.4% SDS, 5% glycerol, and 2 \times TBE. The relaxed DNA and supercoiled DNA were resolved on 1% agarose gel at 75 V for 1.5 h in a running buffer consisting of 50 mM Tris-HCl and 160 mM glycine, pH 7.5. After ethidium bromide staining and fluorescence imaging using a Bio-Rad GelDoc instrument, the bands corresponding to supercoiled and relaxed DNA in each lane were quantified using the software supplied with the instrument. Data were plotted as fraction of relaxed DNA [(counts of relaxed DNA)/(counts of relaxed DNA + counts of supercoiled DNA)] against **[112983]**. Inhibition results using the supercoiled relaxation assay were repeated two times to estimate the variability in the measurements.

Single-Turnover Cleavage Reactions. Inhibition of single-turnover cleavage was investigated using the 2-aminopurine-labeled DNA duplex (FAM-18AP/24) and the 18U-FAM/18-DAB RNase substrate (16). The reactions were performed using an Applied Photophysics stopped-flow fluorescence instrument in the two-syringe mode or, for the RNase reactions, by manual mixing using the Spex Fluoromax 3 fluorometer. Equal volumes of 1 μ M *v*Topo and 50 nM substrate in the presence of 0, 8, or 50 μ M **112983** were rapidly mixed, and the increase in 2-aminopurine fluorescence was followed using excitation at 315 nm with monitoring at emission wavelengths greater than 360 nm using a cutoff filter (14). For the single-turnover RNase reaction, the fluorescence increase of the FAM group was monitored using the same buffer conditions employed in the steady-state RNase measurements. On average, five or more kinetic transients were averaged to obtain the reported rate constants and errors.

Single-Turnover Religation Reactions. Experiments were performed by rapidly mixing a preformed covalent complex with an excess of a 12 mer ligation strand (5' ATTCCGATAGTG 3'). The covalent complex (E-FAM-12/24 mer) was formed by incubating topoisomerase (236 nM) with FAM-18AP/24 (200 nM) for 15 min. The religation reactions (20 μ L total volume) were initiated by rapid mixing of equal volumes of the covalent complex with the complementary 12 mer strand, and the reactions were quenched after 10 s by the addition of loading buffer containing 4% SDS. The final concentrations of the covalent complex and 12 mer were 200 nM and 2.7 μ M, respectively. Reactions were performed in both the presence and absence of 32 μ M **112983**. The E-FAM-12/24 mer covalent complex and the FAM-24/24 mer religation product were separated by electrophoresis using a 15% (w/v) polyacrylamide gel containing SDS. The fractional extent of the covalent complex remaining at a given time (fraction of complex = cpm of complex/total cpm) was quantified using fluorescence imaging with the Image Quant software package provided with the instrument (Typhoon 9410; Amersham Biosciences). The religation measurements were repeated three times to obtain estimated errors.

Equilibrium Cleavage Measurements. The equilibrium cleavage reactions were performed in the presence and absence of compound **112983** (100 μ M) essentially as described previously (14). Wild-type topoisomerase (360 nM) and 5'- 32 P-labeled 40/40 mer DNA (300 nM) with the scissile strand sequence of 5' AACATATCCGTGTCGCCCTTAT-TCCGATAGTGACTACAGC 3' were incubated for 5 min at room temperature, and the covalent complex present at

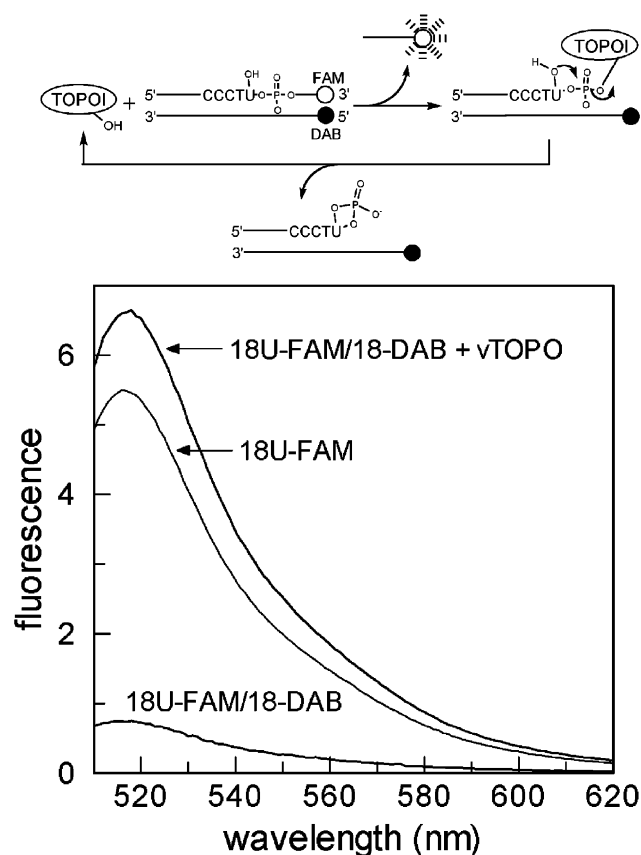


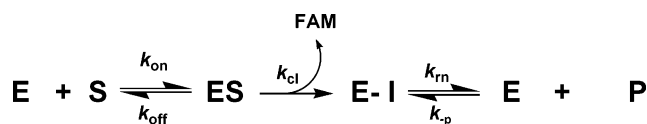
FIGURE 2: Molecular beacon assay for topo I and fluorescence emission spectra for the free molecular beacon substrate and product of the topo I RNase reaction. (Upper graphic) The assay relies on the strong quenching of the 3' 6-carboxyfluorescein fluorophore (FAM) in the substrate by a dabcyI group (DAB) that is covalently attached to the 5' end of the complementary strand. Upon cleavage of the scissile strand by topo I, the short strand with the FAM group is released to solution, resulting in an increase in fluorescence. Recycling of the enzyme for multiple turnovers is accomplished by attack of the 2'-hydroxyl of the uridine ribonucleotide. (Lower panel) The fluorescein emission spectra for the 18U-FAM/18-DAB duplex (50 nM) before (lower spectrum) and after (upper spectrum) 30 min incubation with vTopo. The fluorescence intensity increases by 9-fold when the reaction is completed. The final fluorescence is similar to that of the free 18U-FAM single-stranded DNA (middle spectrum).

equilibrium was trapped by the rapid addition of 1 volume of 5% SDS (20 μ L). The reactions in the presence of **112983** were performed by preincubating the compound with the enzyme or DNA for 5 min before initiating the reaction. The free and covalently bound DNAs were separated by electrophoresis using an 15% polyacrylamide gel containing 0.2% SDS. The fraction of the covalent complex was then determined [fraction of complex = counts of covalent complex/(counts of covalent complex + counts of free DNA)] by phosphorimaging. The equilibrium cleavage measurements were repeated three times for error estimation.

RESULTS AND DISCUSSION

A Continuous Multiple-Turnover Kinetic Assay for Topo I. A molecular beacon substrate was constructed that contained a 6-carboxyfluorescein group (FAM) on the 3' end of the scissile strand and a dabcyI (DAB) quench attached to the 5' end of the complementary strand (Figure 2).

Scheme 1



Cleavage of the scissile strand by topo I was expected to rapidly release the FAM-labeled 6 mer strand to solution, thereby relieving the strong fluorescence quench provided by the DAB group. For this kinetic assay to be mechanistically useful, the release of the 6 mer FAM strand needs to be fast compared to strand cleavage and 2',3'-cyclic phosphodiester formation. It has been previously established that dissociation of an identical 6 mer DNA strand is much faster than the cleavage rate for a DNA substrate containing a CCCTT sequence ($k_{\text{cl}} = 0.7 \text{ s}^{-1}$) (14). As will be shown below, cleavage of a ribonucleotide phosphodiester is 70 times slower than for the preferred DNA substrate, indicating that 6 mer strand dissociation is also not rate-limiting for the RNase reaction.

We investigated the magnitude of the fluorescence increase that occurs upon topo I cleavage of the molecular beacon substrate. Prolonged incubation of 1 μ M substrate with 0.2 μ M topo I resulted in a 9-fold increase in fluorescence at 520 nm (Figure 2). The fold increase in fluorescence at the completion of the reaction was found to be similar to the FAM-labeled single-stranded DNA (18U-FAM, Figure 2), independent of topo I concentration in the range 20–1000 nM and independent of DNA concentration in the range 0.1–3 μ M (not shown). These results indicate that there is a linear relationship between the change in fluorescence and the amount of product formed over a reasonable range of reaction conditions and that the fluorescence measurements can be used quantitatively in mechanistic studies.

Pre-Steady-State Kinetic Analysis of Topo I Ribonuclease Activity. The ribonuclease reaction of topo I occurs by a minimum of three steps involving substrate binding and dissociation to form an ES complex with the rate constants k_{on} and k_{off} , attack of the tyrosine nucleophile to generate a phosphotyrosine intermediate E–I with a rate constant k_{cl} , and release of the enzyme by attack of the 2'-hydroxyl of the uridine ribonucleotide (k_{rm}) to produce the 2',3'-cyclic phosphodiester product as shown in Scheme 1.

Although attack of the 5'-OH leaving group could kinetically compete with k_{rm} , dissociation of the small 6 mer strand is rapid compared to the previously measured religation rate constant ($k_{\text{r}} = 1 \text{ s}^{-1}$) (14). Thus, rapid strand dissociation makes the cleavage step essentially irreversible under these conditions. The final rate constant in Scheme 1 (k_{p}) takes into account that product (P) can accumulate during the reaction assay and may act as a competitive inhibitor with respect to substrate binding to the enzyme. In a pre-steady-state kinetic study, a burst of product formation will be observed when a stable intermediate is formed prior to a slower step on the reaction pathway (17). Under such conditions, the substrate concentration dependence and amplitude of the exponential burst phase provide information on the binding and dissociation rate constants to form ES, as well as the rate constant for formation of the covalent intermediate, E–I. The subsequent linear rate provides information on the rate-limiting turnover of E–I to form free enzyme and product. In contrast, if the rate of intermediate formation is compa-

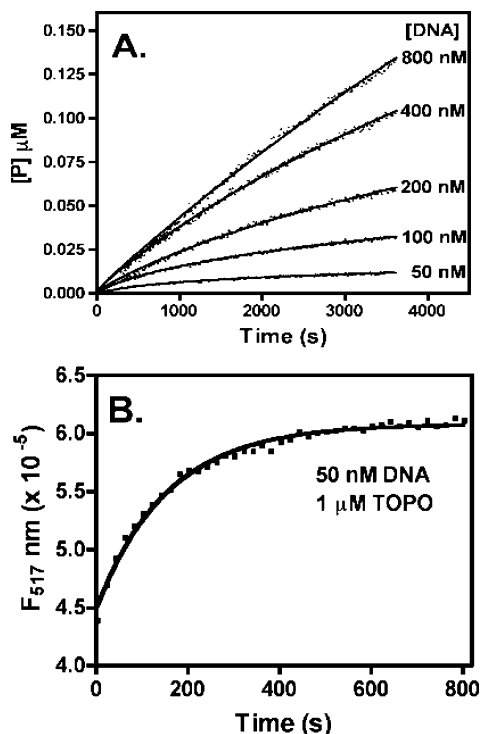


FIGURE 3: Pre-steady-state and single-turnover kinetic analysis of the topo I RNase reaction. (A) Ten nanomolar enzyme was incubated with the molecular beacon substrate at the concentrations indicated in the figure. The solid curves were obtained from global analysis of the time courses using computer simulation and the mechanism shown in Scheme 1. The global best-fit kinetic parameters are reported in Table 1. The kinetic constants in the individual fits that are shown were allowed to float within $\pm 15\%$ of the global values. (B) Single-turnover reaction in which 1 μM vTopo was mixed with 50 nM 18U-FAM/18-DAB duplex. The rate constant obtained from a single-exponential fit to the data was $k_{\text{cl}} = 0.0075 \text{ s}^{-1}$.

able to the rate of the subsequent steps, the burst will be attenuated, and if product inhibition is pronounced, a linear steady-state region will be difficult to measure.

The topo I ribonuclease reaction lacks a clear pre-steady-state burst and linear steady-state region, indicating that the

Table 1: Kinetic Parameters for the Topo I RNase Activity^a

K_D (μM)	k_{on} ($\mu\text{M}^{-1} \text{ s}^{-1}$)	k_{off} (s^{-1})	k_{cl} (s^{-1})	k_{rn} (s^{-1})	$k_{\text{-p}}$ ($\mu\text{M}^{-1} \text{ s}^{-1}$)
0.44	16	7	0.008	$0.008 < k_{\text{-p}} < 0.017$	$0.5 < k_{\text{-p}} < 4$

^a Kinetic parameters were determined at 25 °C in buffer A. Errors for K_D , k_{on} , k_{off} , and k_{cl} were less than $\pm 15\%$. Only a range of values for k_{rn} and $k_{\text{-p}}$ were defined by the data, because k_{rn} is comparable to or greater than k_{cl} , and product inhibition was modest.

rate of formation of the phosphotyrosine intermediate is comparable to the rate of attack of the 2'-hydroxyl group and that product inhibition is significant (Figure 3A). Given the complexity of the kinetic time courses, the data in Figure 3 were fitted by computer simulation to the mechanism shown in Scheme 1 to provide each of the four rate constants as reported in Table 1. Scheme 1 was found to be the simplest model that fits the entire data. The association and dissociation rate constants are similar to the previously reported values for the all DNA cleavage reaction ($k_{\text{on}} = 16 \mu\text{M}^{-1} \text{ s}^{-1}$ and $k_{\text{off}} = 7 \text{ s}^{-1}$) (14). However, the rate constant for attack of the tyrosine nucleophile is 70-fold slower than for an all DNA substrate ($k_{\text{cl}} = 0.008 \text{ s}^{-1}$ for RNA versus $k_{\text{cl}} = 0.7 \text{ s}^{-1}$ for DNA) (14). The calculated k_{cl} value for the RNase substrate determined from the pre-steady-state experiments was directly measured in single-turnover cleavage experiments using the RNase substrate at saturating concentrations of vTopo (Figure 3B, $k_{\text{cl}} = 0.0075 \text{ s}^{-1}$), confirming the reliability of the simulated k_{cl} value (Figure 3B). Because the pre-steady-state assay detects the cleavage and fast release of the FAM-6 mer, the apparent rate constants for the subsequent ribonuclease and product binding reactions were poorly determined by the simulations of the pre-steady-state data. Rate constants for these reactions fell in the range $k_{\text{rn}} = 0.008\text{--}0.017 \text{ s}^{-1}$ and $k_{\text{-p}} = 0.5\text{--}4 \mu\text{M}^{-1} \text{ s}^{-1}$ in the individual simulations of the data shown in Figure 3A (see also Table 1).

Screening the NCI Diversity Library for Topo I Inhibitors. As a test of the molecular beacon assay in a high-throughput application, we screened about one-quarter of the 2000 member Diversity Library available from the NCI. This

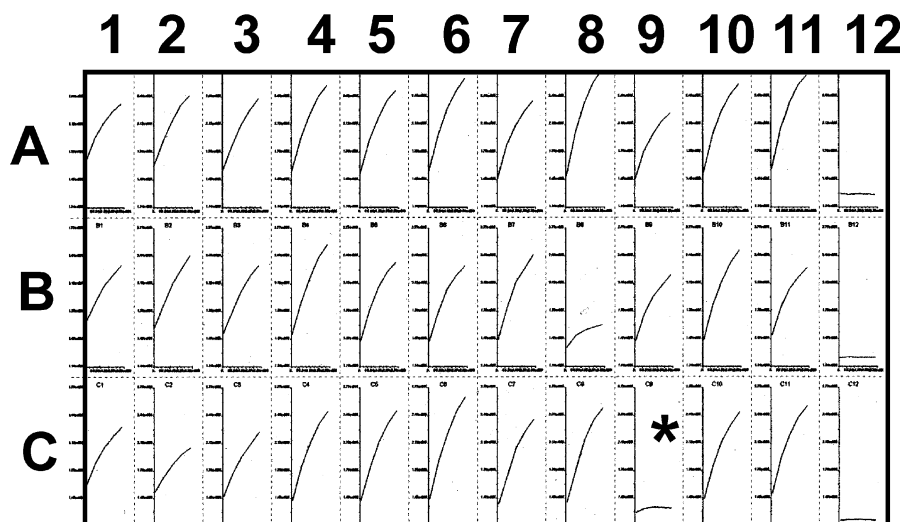
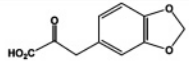
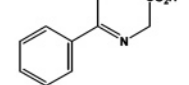
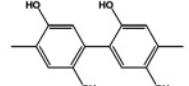
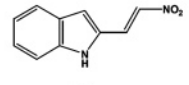
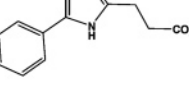
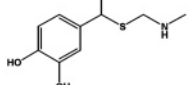
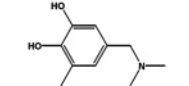
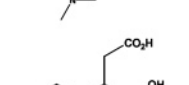
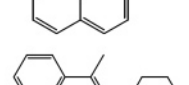
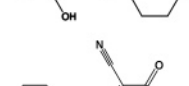
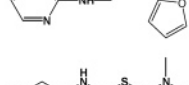
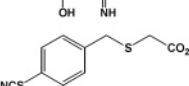
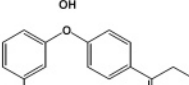


FIGURE 4: Representative inhibitor screening data obtained using the molecular beacon assay and a 96-well microtiter plate format. The figure shows the first three rows of plate 3846 of the NCI Diversity Library Collection. One of the most potent inhibitors detected in our partial screen of this library is compound **112983** (asterisk), which was subjected to further analysis. Column 12 is a negative control (substrate, omit enzyme), and column 1 is a positive control (substrate and enzyme, no compound).

Table 2: Compounds Identified from the NCI Diversity Library as vTopo Inhibitors

NSC Number	Structure	% vTopo RNase activity remaining ^a	% vTopo relaxation activity remaining ^b
112983		9	8
125214		53	10
2805		30	
150982		54	
75600		35	
39215		27	
39225		52	30
163339		48	
120917		28	
379552		7	2
14555		28	
403376		45	
7962		33	

^a Approximately 500 compounds from the library were screened, comprising plate numbers 3843–3847. The screen was performed at $[S] \sim K_m$ and $[I] = 100 \mu M$. The percent activity is compared to that of the enzyme and substrate in the absence of inhibitor. Only compound **112983** was validated in secondary screens and by obtaining an authentic sample from the NCI repository. The other compounds were not subjected to further validation. ^b The inhibition studies were performed using $0.015 \mu g/\mu L$ plasmid, 2 nM vTopo, and $50 \mu M$ compound.

library consists of small molecules that are selected on the basis of a defined set of diversity criteria and are expected

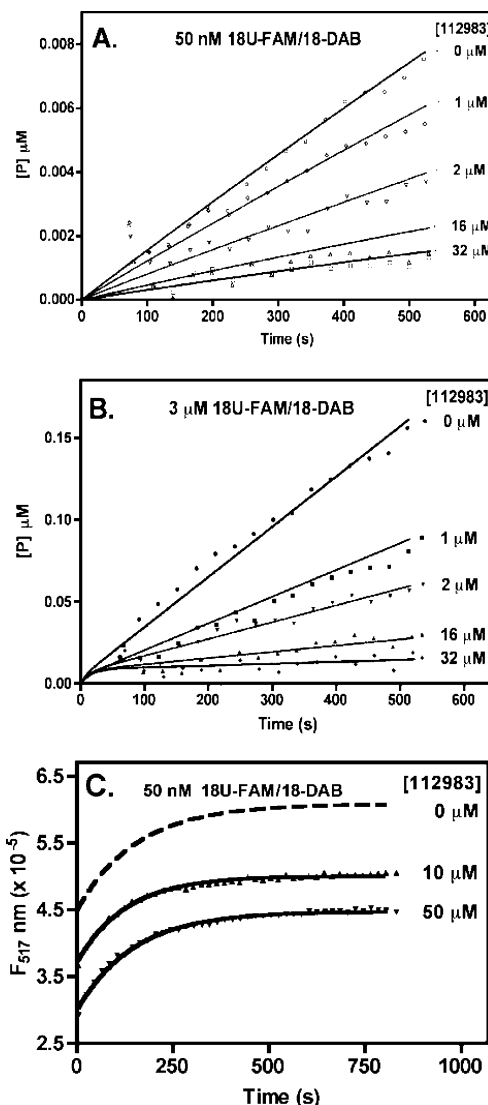
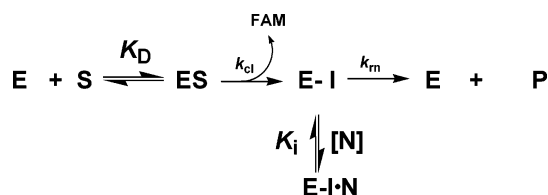


FIGURE 5: Mechanism of inhibition of the topo I RNase activity by compound **112983**. The reactions included 10 nM topo I, either 50 nM (A) or $3 \mu M$ (B) molecular beacon substrate, and the indicated concentrations of **112983**. The solid curves were obtained from global analysis of the time courses using computer simulation and the mechanism in Scheme 2. From this analysis, a K_i value of $1.6 \pm 0.6 \mu M$ for binding of **112983** to the E–I complex was determined. (C) Single-turnover reaction in which $1 \mu M$ vTopo was mixed with 50 nM 18U-FAM/18-DAB duplex in the presence of 0 , 10 , or $50 \mu M$ **112983**. The rate constant obtained from a single-exponential fit to the data was $k_{cl} = 0.0075$, 0.0077 , and 0.0075 s^{-1} for each concentration of inhibitor.

to probe chemical space in an efficient manner. A 96-well format was used in which each well contained 10 nM vTopo, $0.5 \mu M$ substrate, and $100 \mu M$ library compound (see Experimental Procedures), and representative data acquired from three rows of plate 3846 are shown in Figure 4. Using these conditions, a total of 13 compounds were identified that inhibited vTopo activity by greater than 50% (Table 2). Many of the hits showed similar structural features consisting of a substituted phenyl ring that often contained one or more hydroxyl groups. An additional motif that appeared was two fused ring structures or two rings connected by a single or multiple bridging atoms. Two of the compounds (**112983** and **379552**; see Table 2) showed greater than 90% inhibition under these reaction conditions, and compound **112983** was subjected to further mechanistic analysis.

Scheme 2



Mechanism of RNase Inhibition by 112983. To further investigate the mechanism of inhibition, we performed inhibition studies using conditions where the 18U-FAM/18-DAB substrate concentration was much less than and greater than its K_m . The rationale for these conditions is that a competitive inhibitor will show a large increase in its apparent K_i when the assay is performed at high substrate concentrations due to competitive binding effects, whereas if inhibition involves the formation of a ternary complex between E, S, and inhibitor (i.e., noncompetitive or uncompetitive inhibition), the fractional inhibition will be insensitive to substrate concentration. The initial rates of product formation starting from 50 nM and 3 μM 18U-FAM/18-DAB substrate in the presence of increasing concentrations of **112983** are shown in panels A and B of Figure 5, respectively. For both substrate concentrations, 50% inhibition was observed at about 2 μM **112983**, even though the substrate concentrations differed by 60-fold in these two reactions. These results are consistent with an uncompetitive mode of inhibition, requiring that **112983** binds to the covalent complex (E-I, Scheme 2). An alternative noncompetitive mechanism in which N binds to the ES complex would be expected to increase the affinity of S for the enzyme by a mass action effect, which was not observed in trial simulations of the progress curves (not shown) (18). Thus we simulated the progress curves shown in Figure 5 using the simplest mechanism in which **112983** (N, Scheme 2) binds to the E-I covalent complex. This mechanism is most consistent with the data because binding of N occurs after irreversible formation of the E-I complex and, therefore, does not affect binding of S. From these simulations (solid lines, Figure 5), we determined a $K_i = 1.6 \pm 0.6 \mu\text{M}$ for **112983** using the predetermined kinetic constants for the substrate reported in Table 1.

Inhibition of DNA Supercoil Relaxation by vTopo and hTopo. An important question with using the ribonuclease activity to uncover inhibitors is whether the inhibition also extends to the biologically relevant DNA reactions of the enzyme. To address this question, we tested whether **112983** inhibited plasmid supercoil unwinding by vTopo as well as the closely related human topoisomerase IB (hTopo). As shown in Figure 6A, increasing concentrations of **112983** brought about complete inhibition of the supercoil relaxation activity of vTopo. Although these reactions are not carried out under initial rate conditions, 50% inhibition was observed at a concentration of **112983** of about 7 μM . This concentration is similar to the value required to inhibit the ribonuclease reaction by 50%. To test the predictive value of the ribonuclease assay for the discovery of inhibitors of DNA relaxation, we also investigated the inhibition of supercoil relaxation by five other compounds in the NCI library: **120917**, **125214**, **39225**, **379552**, and **14555**; see Table 2. Results using two of these inhibitors are shown in Figure 6A. For a positive control we also tested the weak natural

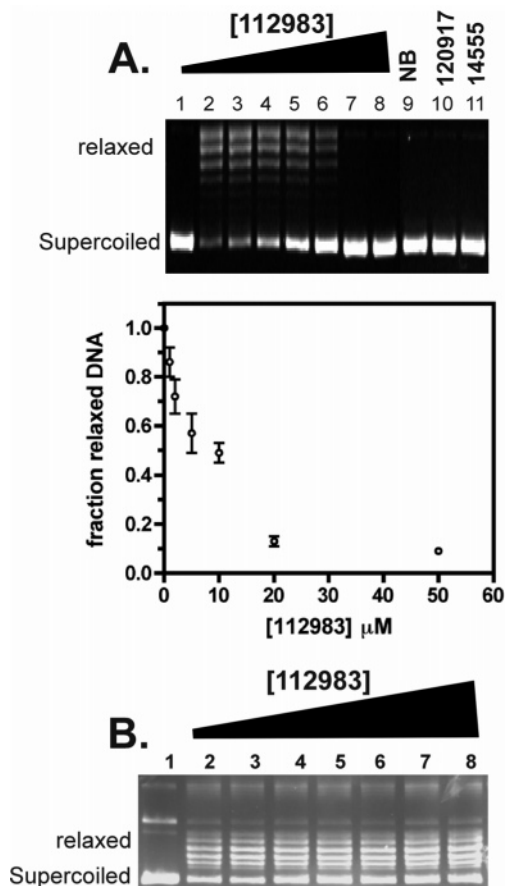


FIGURE 6: Inhibition of DNA supercoil relaxation catalyzed by vTopo and human topoisomerase type IB (hTopo). (A) vTopo and pUC19/AID supercoiled DNA were incubated with increasing concentrations of **112983** for 8 min before the reactions were quenched with 0.4% SDS. The supercoiled and relaxed DNAs were then resolved on a 1% agarose gel and detected with ethidium bromide staining. The relative intensities of the substrate and product bands were determined by fluorescence imaging to calculate the fraction of the DNA in each lane that was in the relaxed form. Lane 1 contains DNA alone; lanes 3–11 contain 3 nM vTopo with **[112983]** = 0, 1, 2, 5, 10, 20, and 40 μM . Lanes 9–11 contain DNA and vTopo plus the following concentrations of inhibitors: lane 9, 1000 μM novobiocin; lanes 10 and 11, 500 μM compound **120917** or **14555**, respectively (see Table 2). The error bars reflect the average of two experiments. (B) hTopo and pUC19/AID supercoiled DNA were incubated with increasing concentrations of **112983** for 15 min before the reactions were quenched with 0.4% SDS. The partially relaxed products were resolved by electrophoresis using a 1% agarose gel. Lane 1 contains DNA alone; lanes 2–8 contain 2 units of hTopo with **[112983]** = 0, 1, 2, 5, 10, 20, and 40 μM .

product inhibitor of vTopo, novobiocin (Figure 6A, lane 9) (19). We found that the inhibitory effects of each of these NCI diversity compounds paralleled their inhibition of the ribonuclease reaction (Table 2) and conclude that the ribonuclease assay reliably detects compounds that are inhibitory to the biologically relevant DNA relaxation reaction. However, for any novel lead this correlation would have to be confirmed.

To investigate the specificity of the observed inhibition, we tested whether the inhibition also extended to supercoil relaxation catalyzed by hTopo (Figure 6B). In contrast to the results with vTopo, increasing the concentration of compound **112983** from 0 to 32 μM resulted in no detectable inhibition of the hTopo reaction. This result excludes the

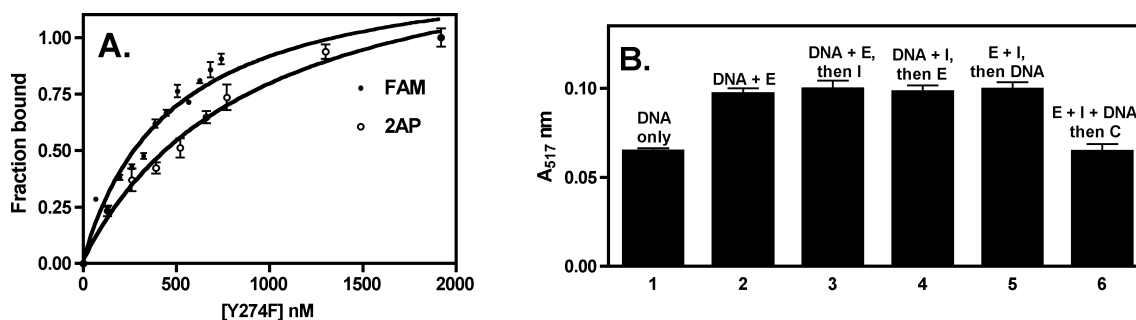


FIGURE 7: Compound **112983** does not inhibit DNA binding of Y274F vTopo. (A) Noncovalent binding of Y274F vTopo to FAM-18AP/24 duplex as monitored by the increase in the steady-state fluorescein anisotropy of the DNA (FAM, filled circles) or increase in 2-aminopurine fluorescence (2AP, open circles). (B) Steady-state anisotropy of (1) the free FAM-18AP/24 mer DNA, (2) the Y274F-FAM-18AP/24 complex, (3–5) the complex in the presence of **112983**, with the order of addition of reagents as indicated, and (6) the complex and **112983** after addition of an unlabeled competitor (C) 24/24 mer duplex (40 μ M) containing a CCCTT consensus sequence.

possibility that **112983** is an indiscriminant protein poison and, instead, indicates that the inhibition by **112983** takes advantage of structural or mechanistic differences between vTopo and hTopo.

Does 112983 Inhibit DNA Binding? The observed inhibition of the RNase and DNA supercoil relaxation activities suggests that binding of compound **112983** is not competitive with the DNA substrate (see above). To confirm these results using another approach, we investigated whether **112983** inhibited noncovalent binding by Y274F vTopo, which lacks the active site tyrosine nucleophile. In this analysis, we followed the change in fluorescence anisotropy upon Y274F binding to the 5'-FAM 18AP/24 duplex (Figure 7A). Addition of increasing concentrations of Y274F to a solution of 5'-FAM 18AP/24 results in a hyperbolic increase in the steady-state fluorescence anisotropy of the DNA (Figure 7A, closed circles), as would be expected upon the formation of a high molecular weight enzyme–DNA complex. The data were fitted to a simple one-site binding equation (eq 1) from which a K_D value of 500 ± 60 nM was calculated. A similar binding constant was determined by following the increase in fluorescence of the 2-aminopurine base (open circles, Figure 7A) ($K_D = 700 \pm 200$ nM). These binding constants are similar to the previously measured K_D for an identical duplex that lacked the 5'-FAM group, establishing that this label does not interfere with the noncovalent interaction of Y274F with the DNA.

To determine if binding of **112983** was competitive with the DNA, we formed a complex between Y274F and 5'-FAM 18AP/24 and monitored the anisotropy as in the presence of **112983** (Figure 7B). At a concentration of compound as high as 32 μ M, the anisotropy was unchanged from that of the enzyme–DNA complex alone (Figure 7B, compare columns 2 and 3). If binding of the compound had displaced the bound DNA, the anisotropy should have returned to the level of the free DNA (Figure 7B, column 1). Changing the order of addition of enzyme, compound, and DNA did not result in a decrease in anisotropy, excluding the possibility that slow onset binding by the inhibitor was influencing the results (Figure 7B, columns 4 and 5). As a positive control, we also added 3 μ M nonfluorescent competitor DNA to the sample containing the complex and compound and observed that the anisotropy returned to the level of the free DNA (Figure 7B, column 6). These data clearly establish that **112983** does not inhibit substrate binding by vTopo.

Does 112983 Inhibit Single-Turnover DNA Strand Cleavage and Religation? The two half-reactions of vTopo (DNA cleavage and religation) can be studied separately using single-turnover conditions. In the cleavage experiment, a “suicide” DNA substrate is employed in which the strand containing the 5'-OH leaving group is sufficiently small that it rapidly dissociates upon cleavage of the phosphodiester linkage (16), resulting in irreversible formation of the covalent complex. If the leaving strand contains a 2-aminopurine fluorescent label on the 5' end, rapid strand dissociation leads to an increase in the 2-aminopurine fluorescence that is a measure of the preceding rate-limiting cleavage reaction (14). In the religation experiment, the covalent complex is first formed using a suicide substrate, and then the ligation reaction is initiated by the addition of a large excess of a complementary DNA strand containing a 5'-OH nucleophile. The extent of ligation may be assessed by electrophoretically separating the covalent complex and ligated DNA using SDS–PAGE (16).

We performed stopped-flow fluorescence analysis of the single-turnover cleavage reaction of the FAM-18AP/24 suicide substrate in the presence of 0, 8, and 50 μ M **112983** (Figure 8A). For comparison, the 50 μ M concentration of **112983** would result in complete inhibition of the steady-state ribonuclease reaction rate (Figure 5A). The cleavage rate in the absence of compound **112983** was 2.03 s^{−1}, which is identical to that previously observed for the 18AP/24 mer that lacked the FAM group (14). The presence of **112983** had no effect on the single-turnover cleavage rate in the concentration range investigated (Figure 8A, lower curve), indicating that inhibition of the steady-state reactions involves a step after formation of the covalent complex. As observed for DNA binding, the results were the same regardless of whether the compound was preincubated with the enzyme or DNA (not shown).

For the single-turnover religation reaction, the covalent complex between vTopo and the FAM-18AP/24 substrate was rapidly mixed with a 12 mer strand in the absence and presence of **112983** (Figure 8B). Ten seconds after initiation the reactions were quenched, and the fraction of covalent complex remaining was determined by separating the complex and DNA ligation product by gel electrophoresis followed by fluorescence imaging. The fraction of covalent complex remaining at the 10 s quench time was decreased by 50% in the presence of 16 μ M **112983**, suggesting that

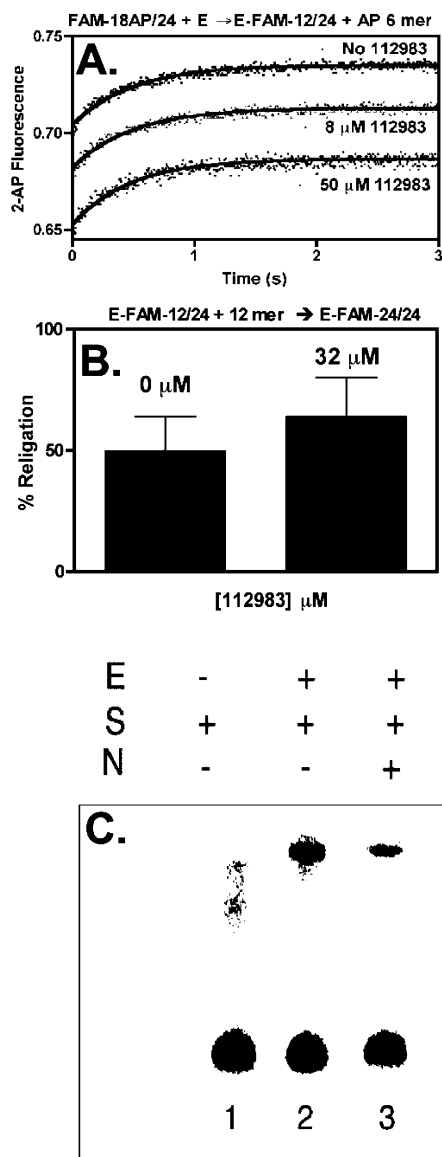


FIGURE 8: Compound **112983** does not inhibit the single-turnover DNA cleavage or ligation reactions of vTopo. (A) Suicide DNA cleavage reaction with fluorescence detection. vTopo was rapidly mixed with a suicide substrate DNA containing a 2-aminopurine fluorescent label in the 6 mer leaving strand (14), and the fluorescence increase was monitored using stopped-flow fluorescence. The cleavage rate was $k_{cl} = 2.03 \pm 0.03$, 2.02 ± 0.03 , and $2.1 \pm 0.05 \text{ s}^{-1}$ in the presence of 0, 8, and 50 μM **112983**, respectively. (B) Single-turnover religation reaction. A covalent complex between vTopo and a 5'- ^{32}P -labeled 12/24 suicide DNA substrate was formed and rapidly mixed with a complementary 12 mer DNA strand that was provided in large molar excess. The 5'-OH of the 12 mer attacks the covalent phosphotyrosine linkage, resulting in the formation of a labeled 24 mer duplex that can be separated from the covalent complex electrophoretically using a 15% SDS–polyacrylamide gel. The ligation reaction was performed in the absence and presence of compound **112983** (32 μM). The reactions were quenched at 10 s, and the percent of the DNA that was covalently bound was determined by phosphorimaging. In the presence of 32 μM **112983**, the percent religation was slightly increased (see text). (C) Equilibrium DNA cleavage. vTopo (360 nM) was added to a solution of 5'- ^{32}P -labeled 40/40 mer (300 nM) and incubated for 5 min before the equilibrium cleavage–religation reaction was quenched by the addition of 5% SDS. The fraction of covalent complex was determined after the free and covalently bound DNAs were separated by gel electrophoresis. The percent covalently bound DNA decreased by 50% in the presence of 100 μM compound (lane 3), further confirming that the compound decreases the cleavage equilibrium (K_{cl}).

this compound alters the cleavage equilibrium (K_{cl}) by increasing k_r ($K_{cl} = [\text{covalent complex}]/[\text{noncovalent complex}] = k_{cl}/k_r$) (Figure 8B). In this analysis, we could have detected a rate decrease of 6-fold given the known half-life of the religation reaction ($\sim 0.7 \text{ s}^{-1}$) (14). As noted below, an *increase* in the rate of religation caused by **112983** would not be detected in this assay but would appear as a decrease in the equilibrium end point because $K_{cl} = [\text{covalent complex}]/[\text{noncovalent complex}] = k_{cl}/k_r$. Thus, the results are consistent with a modest increase in the religation rate induced by **112983**.

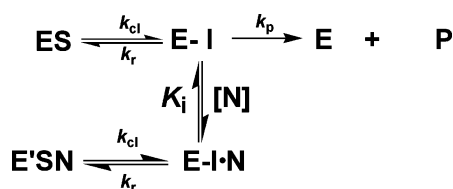
We also further explored whether **112983** affected the overall cleavage equilibrium by performing equilibrium cleavage measurements. In these reactions, vTopo reacts reversibly with a 40/40 mer substrate that has a 5'- ^{32}P label on the scissile strand (16). The equilibrium reaction is rapidly quenched by the addition of SDS, which traps the covalently bound enzyme. Figure 8C shows the extent of equilibrium trapping of covalently bound vTopo in the presence and absence of 100 μM **112983**. In the presence of compound we noted a 2-fold decrease in the amount of covalent complex as compared to a control reaction in the absence of compound. Since **112983** does not inhibit single-turnover cleavage (see above), the observed decrease in the amount of covalent complex formed at equilibrium is consistent with an *increase* in the rate of religation. An increase in the DNA strand ligation rate would act to slow the steady-state RNase and plasmid supercoil unwinding reactions by decreasing the concentration of the reactive intermediate. However, this effect cannot explain the entire inhibitory behavior of this compound because a finite rate would be expected at saturating concentrations of compound, yet the steady-state reactions are completely inhibited (see below).

Mechanism of Inhibition. The above findings indicate that **112983** follows a novel inhibitory mechanism for type IB topoisomerases. This small molecule selectively inhibits the steady-state RNase and supercoil unwinding reactions of vTopo but not hTopo and yet, remarkably, exhibits no detectable inhibition of DNA binding or the single-turnover half-reactions of cleavage and religation (Figures 7 and 8). These observations eliminate two simple mechanisms of inhibition such as competition with substrate binding or targeting of the cleavage chemistry via the formation of an *inhibitory* ESN complex (where N is **112983**). A viable mechanism that is consistent with all of the data is one in which **112983** targets the E–I covalent complex and inhibits attack of the 2'-OH in the ribonuclease reaction and supercoil unwinding with the plasmid substrate (Scheme 3). According to this mechanism, at infinite concentration of **112983**, the equilibrium is shifted completely to the inhibitory EIN

² We note that **112983** has a structure similar to the five- and six-membered C and D rings of camptothecin, with the α -ketocarboxylate moiety resembling the lactone E ring of camptothecin in the open carboxylate form. The significance of these structural similarities is unknown.

³ We have examined the utility of the molecular beacon ribonuclease assay in measuring the ribonuclease activity of the human topo I. Although the human enzyme does not have the sequence preference of vTopo, we had no difficulty detecting a robust signal change for this related enzyme (Nagarajan and Stivers, unpublished results). It is likely that further DNA sequence modifications will significantly enhance the catalytic efficiency of the RNA cleavage reaction for hTopo and make this a very useful assay for hTopo activity as well.

Scheme 3



complex, which is in equilibrium with the E'SN complex. Thus, cleavage and religation are unaffected, but 2'-OH attack and supercoil unwinding are thwarted. The inhibitory mechanism may involve a small stimulation of the religation rate (Figure 8B,C), which would serve to decrease the lifetime of the covalent complex. Shortening the lifetime of the covalent E-I complex inhibits the steady-state RNase and supercoil release reactions because attack of the 2'-OH and strand rotation are competitive with 5'-OH attack (8). A more complicated mechanism that involves binding of **112983** to the E or ES species is not consistent with the data because such binding would lead to an increase in the apparent affinity of S for the enzyme through mass action effects, which is not observed (18). Thus, formation of the noncovalent ES complex follows an ordered mechanism in which **112983** first binds to E-I to form E-IN, and then E-IN is converted to E'SN (Scheme 3). The data do not distinguish whether **112983** exerts its effect by direct interaction at the cleavage site or through binding to an allosteric site. An allosteric mechanism is not unprecedented with vTopo, as nucleoside triphosphates and inorganic pyrophosphate have been found to dramatically stimulate the DNA supercoil relaxation activity of vTopo (20). It is quite possible that the stimulation of DNA ligation by **112983** also arises from an allosteric mechanism.

Comparison with Other Topo I Inhibitors. Type IB topoisomerases can be targeted at multiple points along their reaction pathways ranging from the noncovalent DNA binding step (19, 21), the attack of the tyrosine nucleophile (10, 22, 23), the reverse attack of the 5'-OH (24), and the supercoiled unwinding step (10). Previous studies have shown that DNA binding by vTopo is competitively inhibited by two structurally related antibiotic molecules, novobiocin and coumermycin (19). The inhibition by these molecules is surprising given that they are potent inhibitors of bacterial DNA gyrase enzymes, where they act by binding to the ATP binding sites of these enzymes (25, 26). Like **112983**, novobiocin shows inhibition of vTopo ($K_i = 325 \mu\text{M}$) but no inhibition of the related human topo IB enzyme (8). Other natural product inhibitors of pox virus type IB topoisomerases have been identified (21, 24, 27, 28), but compound **112983** is the simplest yet identified.

Clinically useful drugs that target topoisomerase IB, such as the camptothecin derivatives (29), act by stabilizing the covalent complex and promoting arrest of replication and transcription forks (30). These large five-ring aromatic molecules impose a physical block to ligation by intercalating directly at the cleavage site (31) and are referred to as "poisons" rather than inhibitors of these enzymes. Since compound **112983** does not lead to stabilization of the covalent complex (Figure 8C), it is not a classic topoisomerase poison, although it does exert its effect on the covalent intermediate.² The identification of this compound from a relatively small chemical library suggests that other

novel scaffolds will be found that increase or decrease the level of covalent complex, either through direct or indirect mechanisms. Molecules that act by indirect allosteric mechanisms would be of great interest as potential drugs for treatment of camptothecin-resistant tumors. The high-throughput assay that we have introduced here should greatly accelerate the identification of such potentially useful molecules.³

ACKNOWLEDGMENT

We thank the Developmental Therapeutics Program, DCTD, NCI, for supplying the Diversity Library for these studies.

REFERENCES

- Shuman, S. (1998) Vaccinia virus DNA topoisomerase: A model eukaryotic type IB enzyme, *Biochim. Biophys. Acta* 1400, 321–337.
- O'Brien, P. J., and Herschlag, D. (1999) Catalytic promiscuity and the evolution of new enzymatic activities, *Chem. Biol.* 6, R91–R105.
- Shuman, S. (1992) DNA strand transfer reactions catalyzed by vaccinia topoisomerase I, *J. Biol. Chem.* 267, 8620–8627.
- Christiansen, K., Knudsen, B. R., and Westergaard, O. (1994) The covalent eukaryotic topoisomerase I-DNA intermediate catalyzes pH-dependent hydrolysis and alcoholysis, *J. Biol. Chem.* 269, 11367–11373.
- Krogh, B. O., and Shuman, S. (2000) DNA strand transfer catalyzed by vaccinia topoisomerase: Peroxidolysis and hydroxylaminolysis of the covalent protein-DNA intermediate, *Biochemistry* 39, 6422–6432.
- Sekiguchi, J., and Shuman, S. (1997) Site-specific ribonuclease activity of eukaryotic DNA topoisomerase I, *Mol. Cell* 1, 89–97.
- Werner, R. M., and Stivers, J. T. (2000) Kinetic isotope effect studies of the reaction catalyzed by uracil DNA glycosylase: Evidence for an oxocarbenium ion-uracil anion intermediate, *Biochemistry* 39, 14054–14064.
- Stivers, J. T., Harris, T. K., and Mildvan, A. S. (1997) Vaccinia DNA topoisomerase I: Evidence supporting a free rotation mechanism for DNA supercoil relaxation, *Biochemistry* 36, 5212–5222.
- Liu, L. F., and D'Arpa, P. (1992) Topoisomerase-targeting antitumor drugs: Mechanisms of cytotoxicity and resistance, *Important Adv. Oncol.*, 79–89.
- Liu, L. F., Desai, S. D., Li, T. K., Mao, Y., Sun, M., and Sim, S. P. (2000) Mechanism of action of camptothecin, *Ann. N.Y. Acad. Sci.* 922, 1–10.
- Da Fonseca, F., and Moss, B. (2003) Poxvirus DNA topoisomerase knockout mutant exhibits decreased infectivity associated with reduced early transcription, *Proc. Natl. Acad. Sci. U.S.A.* 100, 11291–11296.
- Summerer, D., and Marx, A. (2002) A molecular beacon for quantitative monitoring of the DNA polymerase reaction in real-time, *Angew. Chem., Int. Ed. Engl.* 41, 3620–3622, 3516.
- Rizzo, J., Gifford, L. K., Zhang, X., Gewirtz, A. M., and Lu, P. (2002) Chimeric RNA-DNA molecular beacon assay for ribonuclease h activity, *Mol. Cell. Probes* 16, 277–283.
- Kwon, K., and Stivers, J. T. (2002) Fluorescence spectroscopy studies of vaccinia type IB DNA topoisomerase. Closing of the enzyme clamp is faster than DNA cleavage, *J. Biol. Chem.* 277, 345–352.
- Kuzmic, P. (1996) Program dynafit for the analysis of enzyme kinetic data: Application to hiv proteinase, *Anal. Biochem.* 237, 260–273.
- Stivers, J. T., Jagadeesh, G. J., Nawrot, B., Stec, W. J., and Shuman, S. (2000) Stereochemical outcome and kinetic effects of Rp- and Sp- phosphorothioate substitutions at the cleavage site of vaccinia type I DNA topoisomerase, *Biochemistry* 39, 5561–5572.
- Fersht, A. (1985) *Enzyme structure and mechanism*, W. H. Freeman, New York.
- Segel, I. H. (1993) *Enzyme kinetics*, John Wiley & Sons, New York.

19. Sekiguchi, J., Stivers, J. T., Mildvan, A. S., and Shuman, S. (1996) Mechanism of inhibition of vaccinia DNA topoisomerase by novobiocin and coumermycin, *J. Biol. Chem.* 271, 2313–2322.
20. Sekiguchi, J., and Shuman, S. (1994) Stimulation of vaccinia topoisomerase I by nucleoside triphosphates, *J. Biol. Chem.* 269, 29760–29764.
21. Hwang, Y., Rowley, D., Rhodes, D., Gertsch, J., Fenical, W., and Bushman, F. (1999) Mechanism of inhibition of a poxvirus topoisomerase by the marine natural product sansalvamide A, *Mol. Pharmacol.* 55, 1049–1053.
22. Pilch, D. S., Xu, Z., Sun, Q., LaVoie, E. J., Liu, L. F., and Breslauer, K. J. (1997) A terbenzimidazole that preferentially binds and conformationally alters structurally distinct DNA duplex domains: A potential mechanism for topoisomerase I poisoning, *Proc. Natl. Acad. Sci. U.S.A.* 94, 13565–13570.
23. Rangarajan, M., Kim, J. S., Sim, S. P., Liu, A., Liu, L. F., and Lavoie, E. J. (2000) Topoisomerase I inhibition and cytotoxicity of 5-bromo- and 5-phenylterbenzimidazoles, *Bioorg. Med. Chem.* 8, 2591–2600.
24. Hwang, Y., Rhodes, D., and Bushman, F. (2000) Rapid microtiter assays for poxvirus topoisomerase, mammalian type IB topoisomerase and HIV-1 integrase: Application to inhibitor isolation, *Nucleic Acids Res.* 28, 4884–4892.
25. Celia, H., Hoermann, L., Schultz, P., Lebeau, L., Mallouh, V., Wigley, D. B., Wang, J. C., Mioskowski, C., and Oudet, P. (1994) Three-dimensional model of escherichia coli gyrase B subunit crystallized in two-dimensions on novobiocin-linked phospholipid films, *J. Mol. Biol.* 236, 618–628.
26. Lewis, R. J., Singh, O. M., Smith, C. V., Maxwell, A., Skarzynski, T., Wonacott, A. J., and Wigley, D. B. (1994) Crystallization of inhibitor complexes of an N-terminal 24 kDa fragment of the DNA gyrase B protein, *J. Mol. Biol.* 241, 128–130.
27. Hwang, Y., Wang, B., and Bushman, F. D. (1998) Molluscum contagiosum virus topoisomerase: Purification, activities, and response to inhibitors, *J. Virol.* 72, 3401–3406.
28. Yakovleva, L., Handy, C. J., Sayer, J. M., Pirrung, M., Jerina, D. M., and Shuman, S. (2004) Benzo[c]phenanthrene adducts and nogalamycin inhibit DNA transesterification by vaccinia topoisomerase, *J. Biol. Chem.* (in press).
29. Hsiang, Y. H., Liu, L. F., Wall, M. E., Wani, M. C., Nicholas, A. W., Manikumar, G., Kirschenbaum, S., Silber, R., and Potmesil, M. (1989) DNA topoisomerase I-mediated DNA cleavage and cytotoxicity of camptothecin analogues, *Cancer Res.* 49, 4385–4389.
30. Hsiang, Y. H., Lihou, M. G., and Liu, L. F. (1989) Arrest of replication forks by drug-stabilized topoisomerase I-DNA cleavable complexes as a mechanism of cell killing by camptothecin, *Cancer Res.* 49, 5077–5082.
31. Staker, B. L., Hjerrild, K., Feese, M. D., Behnke, C. A., Burgin, A. B., Jr., and Stewart, L. (2002) The mechanism of topoisomerase I poisoning by a camptothecin analogue, *Proc. Natl. Acad. Sci. U.S.A.* 99, 15387–15392.

BI048801S